Laser-induced magnetic fields in ICF capsules
Final Report, DE-FG02-08ER85128, Phase 1

E.L. Lindman

Otowi Technical Services, Los Alamos, New Mexico, USA

Abstract

The advantages of inserting a magnetic field into an inertial-confinement-fusion (ICF) capsule before compressing it have been pointed out by many authors. A mechanism for generating such a field without the use of low-inductance electrical conductors attached to the capsule is presented. To use this mechanism to insert a magnetic field into an ICF capsule, the capsule must be redesigned. In our approach, a central conductor is added, a toroidal gap is cut in the outer wall and the DT fuel is frozen on the inner surface of the capsule. The capsule is dropped into the reaction chamber and struck first with the laser that generates the magnetic field. The magnetic field propagates into the interior of the capsule through the toroidal gap, and the main compression then closes the gap, crowbars the field, and compresses the fuel to ignition. Other uses of this mechanism include the generation of large magnetic fields in laboratory apparatus for the measurement of the effects of magnetic fields on material samples.

PACS
52.35.Fp – Electrostatic waves and oscillations in plasmas
52.38.Fz – Laser-induced magnetic fields in plasmas
52.38.Kd – Laser-plasma acceleration of electrons and ions
52.57.Bc – Laser-inertial-fusion-target design and fabrication

Keywords
Resonant absorption
Hot electrons
Mega-gauss magnetic fields
Magneto-inertial fusion

1. Introduction

The advantages of inserting a large magnetic field into an inertial-confinement-fusion (ICF) capsule before compressing it have been pointed out by many authors[10-12,1,2,5]. A comprehensive presentation of the subject can be found in the overview [10] by R. C. Kirkpatrick, et al. Among the advantages, the suppression of electron thermal-conduction losses is, perhaps, the most important, but the control of alpha-particle energy deposition has received some attention as well [13,17]. The scientific community is also interested in the generation of large magnetic fields in the laboratory in order to evaluate the effects of such fields on plasmas similar to astrophysical plasmas and on material samples. Currently, the largest experimentally observed magnetic fields have been generated in experiments involving laser interaction with matter. Fields as high as 0.35 to 0.7 Giga gauss have been inferred from an analysis of the harmonic emission that comes from the laser-matter-interaction region [20] and fields as high as

3 Mega gauss have been observed using Faraday rotation as the diagnostic [4]. The fact that these extraordinarily impressive field strengths are still 5 or 6 orders of magnitude smaller than the fields in magnetars suggests that we have a long way to go to address issues of interest to many astrophysicists.

Unfortunately, these magnetic fields cannot be inserted into an ICF capsule or used to measure the effects of a magnetic field on a material sample. They were obtained in experiments using ultra-intense lasers in which the intensity of a Nd-YAG laser (usually doubled or tripled in frequency) is amplified by shortening the pulse [9]. More extreme conditions can be obtained by shortening the pulse further or by shortening the pulse of a more intense glass laser. But there are serious problems with using these magnetic fields to do laboratory experiments. First, the size of the experimental region is the laser-spot size. It is comparable to the wavelength of the laser (1.05 to 0.35 μm) and is therefore too small. Second, the time over which the fields exist is the pulse length (1 ps or less) and it is too small as well. A limited class of experiments can be carried out within these constraints on space and time. Third, in addition to the desired magnetic fields, there are intense laser electric and magnetic fields present in the experimental region. Sorting out which effects are caused by the desired magnetic field and which are the result of the high-frequency laser fields is very difficult. And fourth, there are large numbers of relativistic electrons present. Sorting out which effects are caused by the desired magnetic field and which are caused by the hot electrons is also very difficult. These four issues suggest that an alternative method is needed to address the applications of interest.

The ICF application suggests an alternate strategy for the other applications. In it, the largest magnetic field possible is induced in a liner or capsule containing plasma and then this "seed" field is amplified by compressing the capsule. Technologies, already available for magneto-inertial fusion such as those being investigated at the National Ignition Facility at Lawrence Livermore National Laboratory, at the Laboratory for Laser Energetics at the University of Rochester and at the Z machine at Sandia National Laboratories, can be used for the compression. The technology to be used to inject the seed field into the capsule remains unspecified.

One approach, under investigation by Ricardo Betti [3] at the University of Rochester, is the redesign of inertial-fusion capsules to include electric conductors that are attached to an external capacitor bank. The capacitor bank is then discharged to induce the magnetic field in the capsule before firing the laser to compress the capsule. This approach easily overcomes the four disadvantages listed above for ultra-intense lasers. It has two serious disadvantages, however. First, the maximum seed magnetic field that is accessible is probably less than 100 kilogauss. And second, there is no standoff. In a magneto-inertial-fusion (MIF) power generator, one would prefer to drop capsules into the reactor volume, with no low-inductance electrical connections attached [18], and compress them with the laser.

2. A laser-generated seed field

We suggest an alternate approach in which a laser is used to induce the currents and magnetic field in a capsule. It is based on experimental work that was first carried out at Gifu University in Japan [19]. In these experiments, a low-intensity Nd-YAG laser was used to irradiate a target

made of audio magnetic tape. A nearly circular burn pattern was seen on the tape, but the observed magnetic field showed a non-circular magnetic structure with a magnetic field that was perpendicular to the plane of incidence of the laser beam. The magnetic field was in opposite directions on either side of the spot with a null along a line through the center of the spot perpendicular to the plane of incidence. Kolodner and Yablonovitch [14] suggested that this magnetic-field pattern was consistent with the acceleration of hot electrons by the non-circular laser-field patterns expected in resonant absorption.

Subsequent experimental and simulation work was carried out with a high-intensity CO_2 laser at the Los Alamos National Laboratory (LANL) [23]. Resonant absorption was identified as the dominant laser-light absorption mechanism [6,7]. The energy was deposited into a current of hot electrons that was ejected out of the plasma toward the vacuum. The current of hot electrons also generated a magnetic field. This magnetic field was part of a stable structure (shown in Figure 1) that extended millimeters from the hot spot. It prevented the hot electrons from depositing all of their energy in the laser hot spot. Instead the hot-electron energy was deposited over a millimeter-size region occupied by the magnetic field. This region appeared to be circular, suggesting that the magnetic-field structure was toroidal.

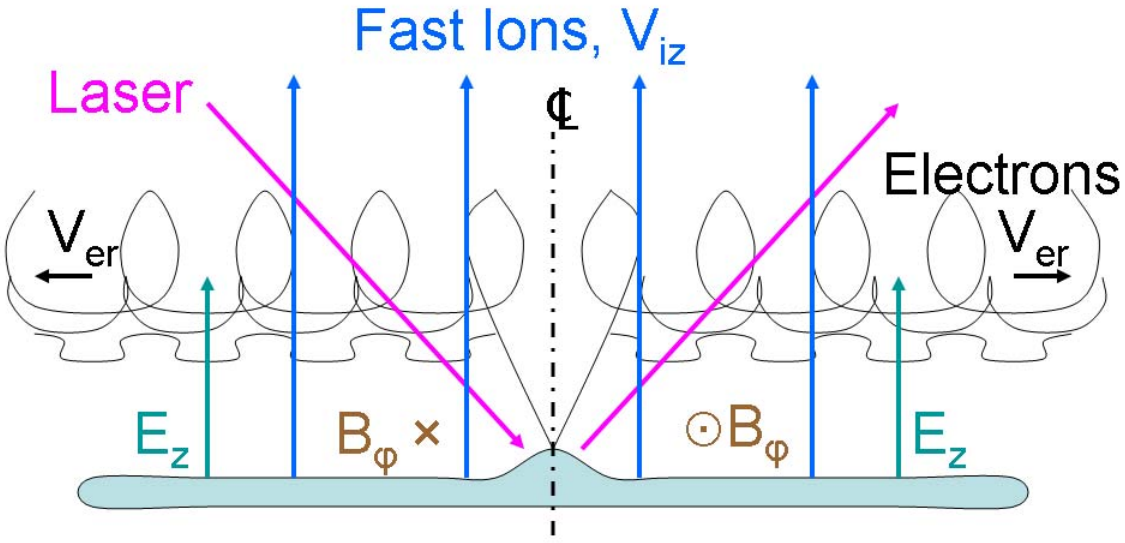

Figure 1. A p-polarized (electric field in the plane of incidence of the laser beam with a component normal to the target surface) CO_2 laser beam strikes a material surface and is reflected. The material in the hot spot is ionized and hot electrons are emitted normal to the surface. A self-consistent structure forms with an electric field that is normal to the surface in the z direction, a magnetic field that is parallel to the surface in the φ direction and hot electrons that ExB drift in the radial direction. Fast ions are also accelerated normal to the surface.

These experimental results are unique. They are the only results reported in the literature in which a magnetic field is generated well outside of the laser spot by laser interaction with matter.

The space scale of the magnetic field is millimeters. The time scale in these experiments is nanoseconds. And there are no laser electric and magnetic fields in the region occupied by the magnetic field. With three of the four issues, identified above, eliminated, this approach has merit and should be pursued.

When these experimental results were obtained, there was no interest in magnetic fields. The research program (see Appendix 1 for more details) was focused entirely on using lasers to compress inertial-fusion capsules. As a result many issues with regard to the magnetic fields remain unanswered.

First, there were no experimental measurements of the magnetic field strength. Instead estimates were obtained from computer-simulation studies [22]. The computer code available at the time was non-relativistic, so simulations were limited to intensities that led to non-relativistic hot-electron temperatures. At intensities of 5×10^{13} W cm^{-2}, hot-electron temperatures of 20 keV were experimentally measured. Using these temperatures in the simulation studies, magnetic field strengths of 0.5 Mgauss were obtained 150 μm from the spot center. The magnetic-field strength was observed to decrease with radius from the hot spot in proportion to r^{-1} as expected. In experiments performed at intensities of 10^{16} W cm^{-2}, the measured hot-electron temperature was 200 keV and the magnetic-field effects were more pronounced. A simple scaling argument (see Appendix 2) suggests that the magnetic fields expected at 10^{16} W cm^{-2} should be 9 Mgauss, a factor of 18 larger than those obtained at 5×10^{13} W cm^{-2}.

Second, there were no attempts to optimize the magnetic field strength. In the simulations it was assumed that the critical surface remained parallel to the original flat surface and, consequently, that the hot electrons were ejected in a cone within 20º degrees of the target normal. Only the self-electric field of the hot electrons was available to give the electrons a component of velocity in the radial direction parallel to the target surface. A large fraction of the ejected electrons (80 to 90%) fell back into the hot spot canceling the current supporting the magnetic field. It was far more likely that the critical surface was either concave or convex. In either case the hot electrons would have been ejected into a larger cone of angles. This effect should be included and could be further enhanced by appropriate adjustments of the shape of the target surface at the laser hot spot and adjustments of the orientation of the laser beams.

Third, there was no attempt to optimize the extent to which magnetic insulation [8] kept the hot electrons away from the target surface outside the hot spot. Magnetic insulation arises because the motion of the electrons is determined by ExB drift and the electric field near the surface of a conductor is normal to it. Thus, in a sufficiently strong magnetic field, the electrons move parallel to the surface of a conductor and they are prevented from striking the surface. When the magnetic field weakens, it can no longer hold them out and they deposit their energy in the surface.

Some indirect evidence for a strong magnetic-insulation effect was seen in experiments in which two laser hot spots spaced 1mm apart were irradiated simultaneously [23]. The surface damage was minimal outside the two laser spots except in a region half-way between them, where it was quite large. In the region half-way between them, the magnetic fields generated by the hot

electrons from the two spots were predicted to cancel, and the magnetic insulation should no longer protect the surface from damage.

Fourth, there was no attempt to measure the effects of a background plasma on the magnetic field and the fast-ion losses. The density of such a plasma would have to be less than the critical frequency of the CO_2 laser (10^{19} cm^{-3}) to allow the laser energy to reach the hot spot. As the hot electrons move away from the hot spot, they would sweep the cold plasma electrons out of the region. The electric field of the hot electrons would then be partially neutralized by cold stationary ions rather than fast ions with no change in the magnetic field. This neutralization may help in the optimization of the structure when a high-atomic-mass material without hydrogen-surface contamination is used.

The fact that the electrons move in a direction parallel to a conducting surface and stay close to it, even if it is curved [23], leads to potential target-design features that can be quite useful. Target designs that take advantage of this fact are shown in Figures 2 and 3. Both include a gap in the structure through which the magnetic field and the electrons may move. If the gap is large enough, the second conducting surface is too far away to modify the electric field that the electrons see and they move along the surface into the interior of the target. As the gap becomes smaller, the electrons may jump the gap and move along the exterior surface of the target. In either case, the magnetic field moves through the gap and into the interior of the target.

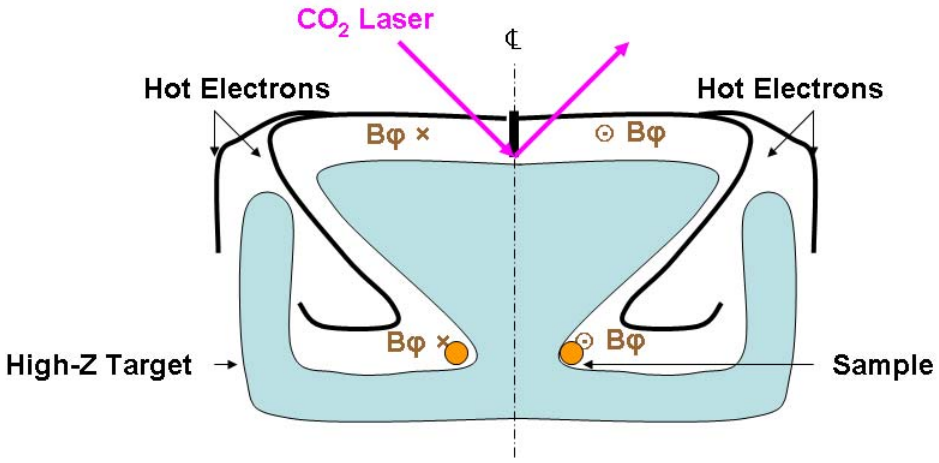

Figure 2. A p-polarized CO_2 laser beam strikes a material surface and is reflected. The material in the hot spot is ionized. Hot electrons are emitted normal to the surface and accelerated along the surface by their self field. The hot electrons follow the curvature of the surface. Some go through the gap and enter the interior region. Others jump the gap and follow the external surface.

The target design, shown in Fig. 2, is a preliminary design for experiments on the effects of magnetic fields on material samples. It is made of high-density material with no hydrogen surface contamination to minimize fast ion losses and to minimize x-ray preheat of the sample

(the material, whose magnetic properties are to be measured). In it, the gap is designed to allow the magnetic field to move into the interior of the target while minimizing the flow of hot electrons into the interior. By adjusting the size and orientation of the gap as well as its surface structure, the hot-electron effects can be minimized. Since the strength of the magnetic field depends on the radial distance to the sample from the center of the conductor carrying the return current, the sample is located at a point of minimum conductor radius. This location also minimizes the effects on the measurement of any hot electrons that flow into the interior. Useful experiments can be accomplished with the "seed" field alone in this geometry. Compressing the capsule after the insertion of the seed field may allow experiments with even larger magnetic fields.

The target design, shown in Fig. 3, is a preliminary design for magneto-inertial fusion. Here we would like the hot electrons to enter the interior to provide fast-ion and resistive heating of the plasma in addition to the magnetic field. After the magnetic field is established, the capsule is to be compressed. During this compression the gap is designed to close and "crowbar" the field. The field strength will then rise as expected inside the conducting walls of the capsule. The central conductor is designed with a notch in it. This notch is a seed for the "sausage" instability which is designed to grow and remove the central conductor from the central region of the compressed plasma. Techniques for inducing a poloidal field should be included in the final design, as well.

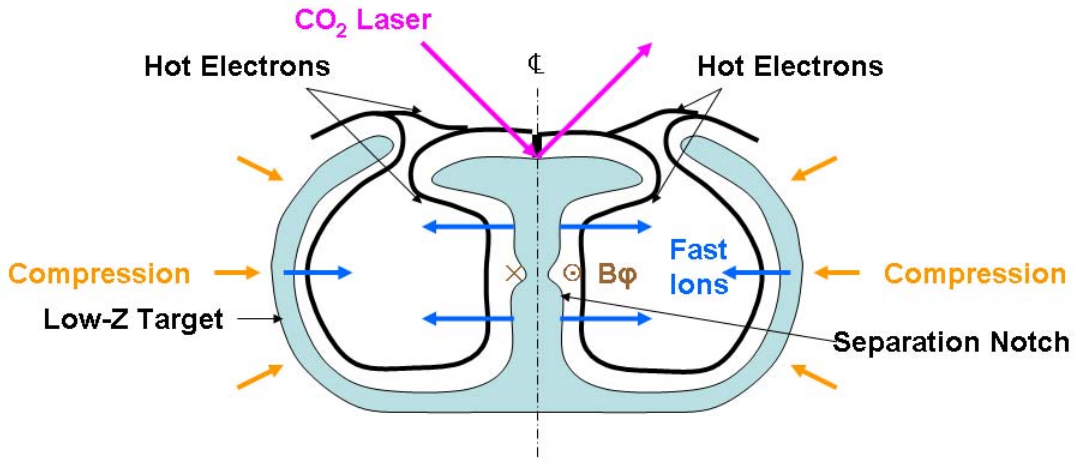

Figure 3. A p-polarized CO_2 laser beam strikes a material surface and is reflected. The material in the hot spot is ionized. Hot electrons are emitted normal to the surface and accelerated along the surface by their self field. The hot electrons follow the curvature of the surface. Some go through the gap and enter the interior region. Others jump the gap and follow the external surface.

Experimental [23] and computational [8,22] evidence for the existence of this magnetic field have been published, but no one has shown that the magnetic field and/or the hot electrons will go through a gap into the interior of a target such as those shown above. Consequently, our recent computational work has been focused on demonstrating this effect. We have also evaluated some of the suggested procedures for enhancing this magnetic-field-generation mechanism.

In our current work we do not attempt to calculate the dynamics of resonant absorption. Instead, (as others have done [8,22]) a cylindrical region is defined just inside the high-density plasma that has a diameter equal to that of the hot spot and an arbitrary depth. In every time step, an appropriate number of electrons are selected at random from within this region and converted to hot electrons by accelerating them. In our case, they are accelerated into a relativistic-Maxwellian [16] distribution within a cone of angles normal to the surface.

3. Calculation 1

The initial plasma for Calculation 1 is shown in Fig. 4. The high-density structure consists of a slab of plasma on a pedestal with a rounded edge and an elliptical void. The high-density region has a density that is twice critical ($n_{crit} = 10^{19}$ cm^{-3}) and is immersed in a background plasma with a density of 0.071 critical. The elliptical void has sharp corners and a narrow gap through which electrons and/or magnetic field can penetrate. The rounded outer surface is designed to show the propagation of the electrons and the magnetic field around a smooth, gently curved surface.

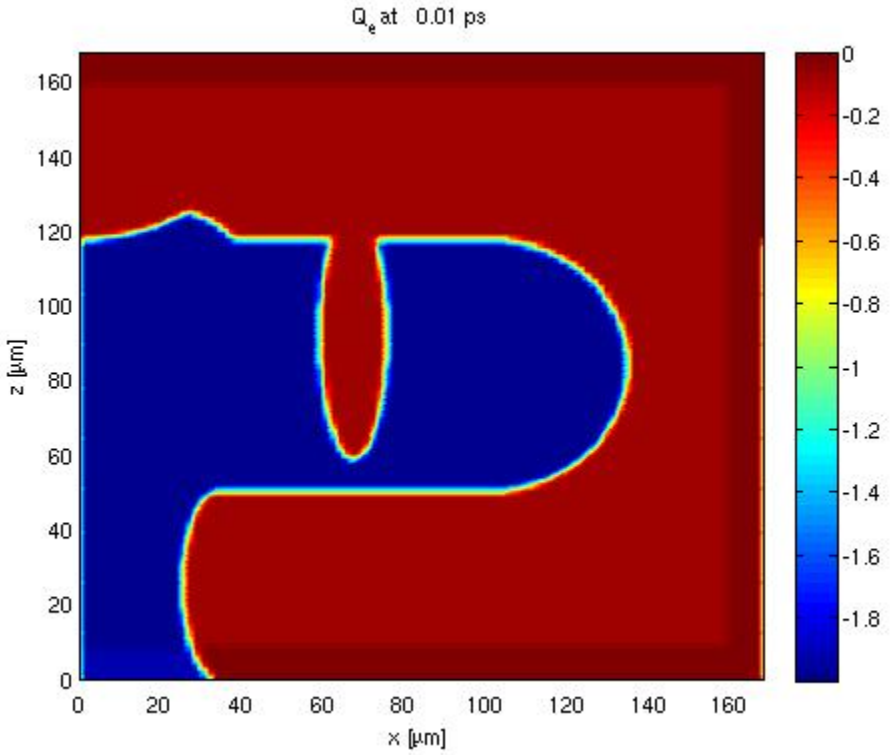

Figure 4. The initial plasma geometry for Calculation 1.

The calculation is done in Cartesian coordinates with the CELESTE code [15] and the left boundary is a symmetry boundary. The ions are mass-100 ions (A=100) to minimize plasma motion during the calculation. The hot-electron generation region has a half width of 33.6 μm, is centered on the left boundary and its upper boundary coincides with the upper boundary of the

high-density plasma slab. The curved structure near the hot-electron-generation region is designed to mimic the structure induced in the plasma by the ponderomotive force and to reflect lower-energy hot electrons straight down and maximize their removal from the system. Hot electrons that strike the bottom boundary are converted back to cold electrons. Open boundaries are not available in hybrid codes so reflecting or periodic boundaries are used and the phenomena of interest must always be clearly separated from the boundary. The calculation was done with 27 particles per cell at high density and a rise time of 12 ps was used to turn on the electron accelerator. Out put from the calculation at 13.5 ps, shortly after attaining full heating power, is shown in Fig. 5.

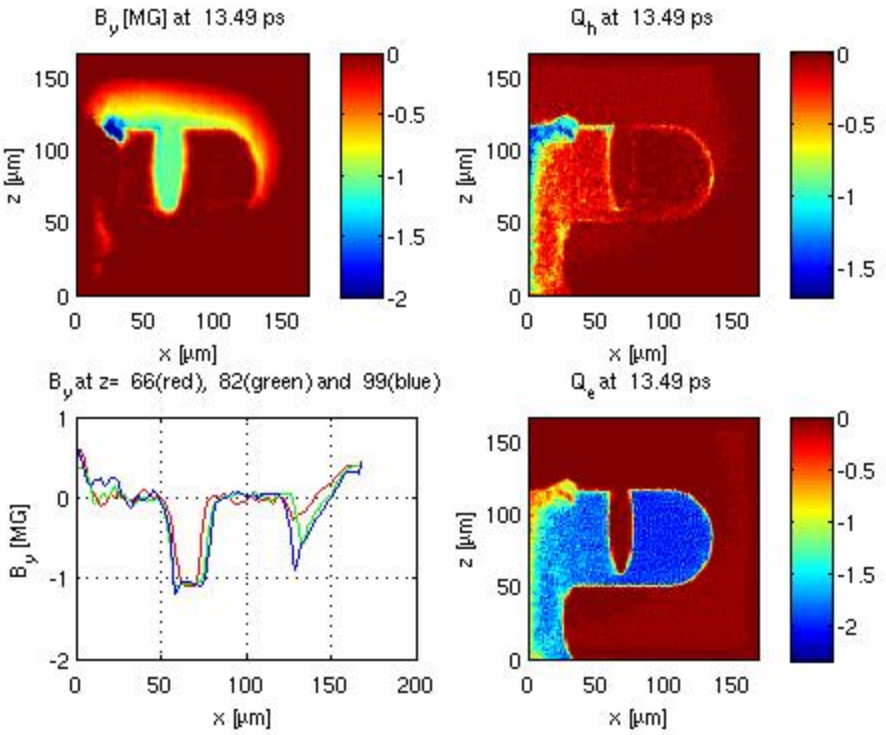

Figure 5. Calculation 1 at 13.5 ps

The y component of the magnetic field is shown in the color contour plot at the upper left. Hot electrons are generated inside the high-density structure at the upper left, reflect off the symmetry boundary and propagate along the surface generating a magnetic field between 1 and 2 Mg. Most, but not all, jump the gap at the top of the elliptical void. Since most of the electrons jump the gap, the magnetic field in the elliptical gap is quite uniform with only a hint of additional field at a few spots. Having jumped the gap, the electrons easily follow the smooth contour of the outer boundary of the slab.

In the upper right-hand color contour plot, the spatial density of electrons that are tagged as "hot electrons" is shown. The strong electric fields, that occur and E×B drift the electrons through the magnetic field, reflect the lower-energy accelerated electrons in the thermal distribution. These electrons are still tagged as hot electrons and remain in the calculation until they strike the

bottom boundary. The result of this effect is a gradual buildup of hot electrons in the calculation as shown. As previously discussed, the ions do not move, so the increase in hot electrons is matched with a decrease in the number of cold electrons as shown in the lower right-hand plot.

These calculations support the claim that the electrons can jump a gap while the magnetic field goes through the gap and fills the void. And that the hot electrons can easily follow a gently curved surface and bring the field along with them.

Fig. 6 shows output from the calculation at 27 ps. At this time, there are regions where hot electrons have completely replaced the colds. It is also clear that the "elliptical volume" occupied by the magnetic field is much larger than the elliptical volume defined by the plasma which has not moved.

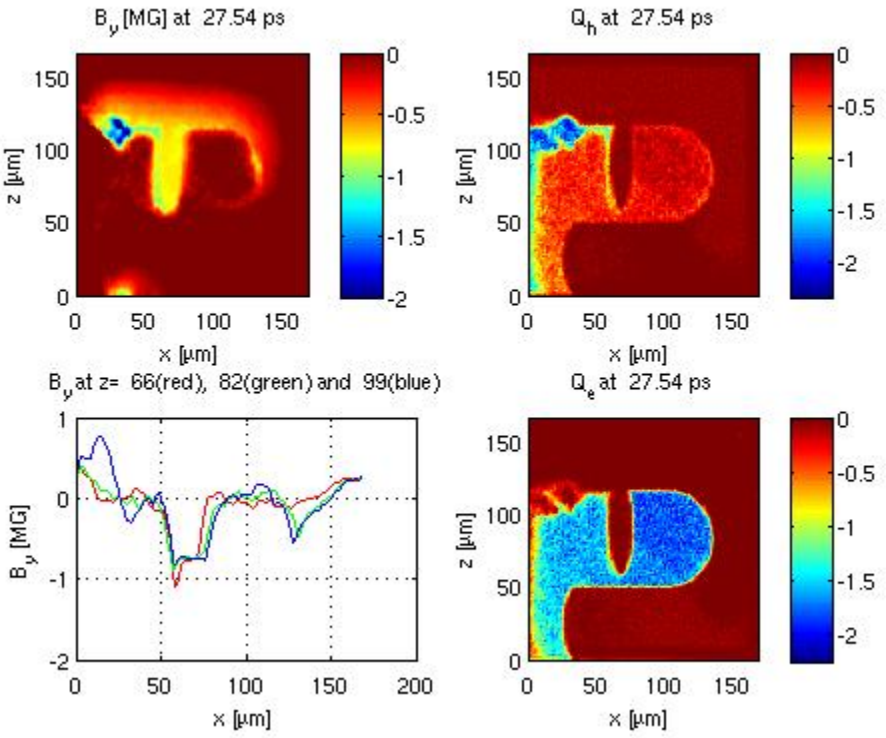

Figure 6. Calculation 1 at 27ps.

This result suggests that the magnetic field is being transported into the high-density plasma. There are two possible mechanisms for this transport. Numerical collisions may allow diffusive transport into the high-density region (see Appendix 3 for a discussion of this effect). But, the transport equation also contains a term describing the transport of the field that is "frozen into the electrons" by the motion of the electrons. If magnetic-field-free electrons can be moved out of the way, then electrons carrying a frozen-in field can move in bringing their field with them. It is quite possible that both mechanisms are at work.

Output from Calculation 1 at 56 ps is shown in Fig. 7. Hot electrons now move easily through the gap and enter the elliptical volume. The magnetic field strength which had dropped to 0.5 Mg has now returned to 1 Mg. The dynamics are quite complicated and additional diagnostics are required to sort out the important physics.

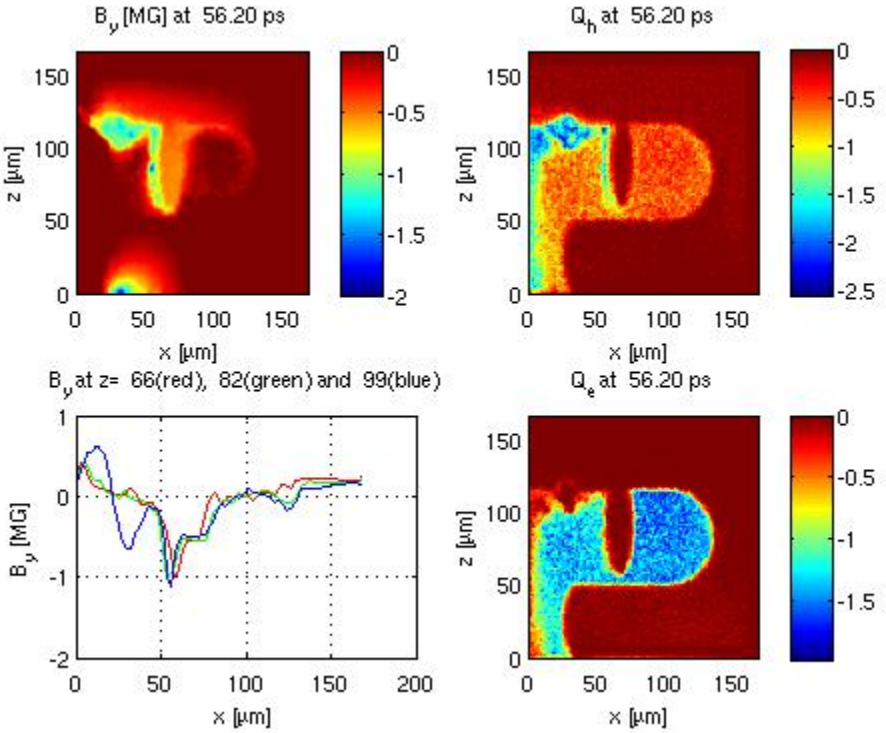

Figure 7. Calculation 1 at 56 ps.

4. Calculation 2.

We have also studied a second geometry with a larger gap that allows the hot electrons to enter the interior region along with the magnetic field. The initial plasma geometry is shown in Fig. 8. Here the dense-plasma region is a quasi-cylindrical shell in contact with a symmetry boundary on the left and a particle-conversion boundary on the bottom. Electrons and magnetic field have access to a large cylindrical internal region through a large gap with rounded edges in the boundary. The high-density region has a density that is twice critical and is immersed in a background plasma with a density of 0.071 critical.

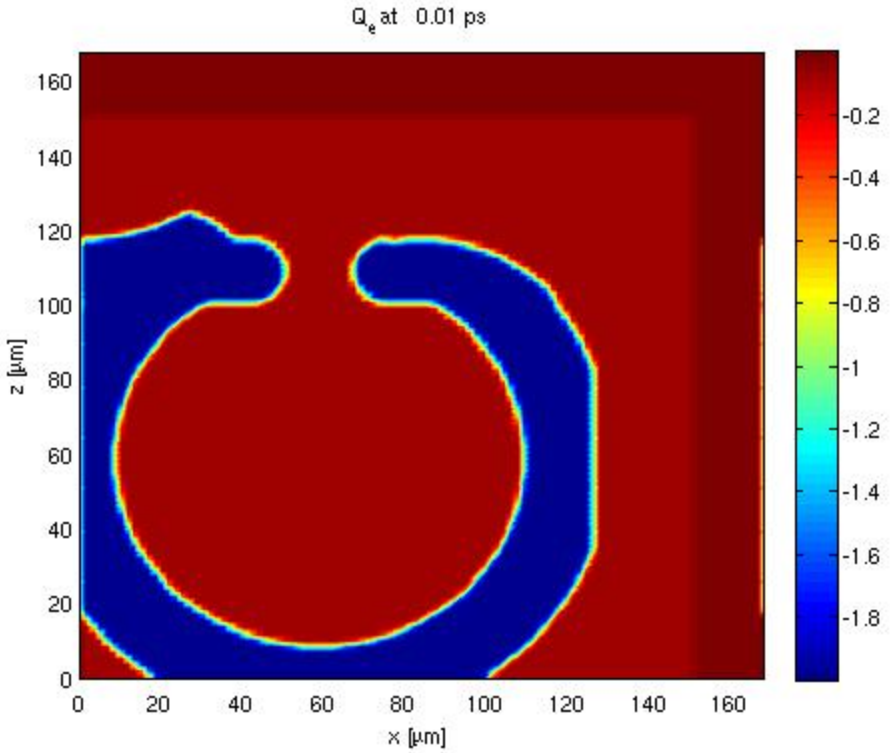

Figure 8. The initial plasma geometry for Calculation 2.

The calculation was done in Cartesian coordinates and the ions are mass-100 ions (A=100) to minimize plasma motion during the calculation. The hot-electron generation region has a half width of 33.6 μm, is centered on the left boundary and its upper boundary coincides with the upper boundary of the high-density plasma slab. The curved structure is designed to mimic the structure induced in the plasma by the ponderomotive force and to reflect lower energy hot electrons straight down and maximize their removal from the system. Hot electrons that strike the bottom boundary are converted back to cold electrons. Open boundaries are not available in hybrid codes so reflecting or periodic boundaries are used and the phenomena of interest must always be clearly separated from the boundary. The calculation was done with 27 particles per cell at high density and a rise time of 12 ps was used to turn on the electron accelerator. Output from the calculation at 13.5 ps, shortly after attaining full heating power, is shown in Fig. 9.

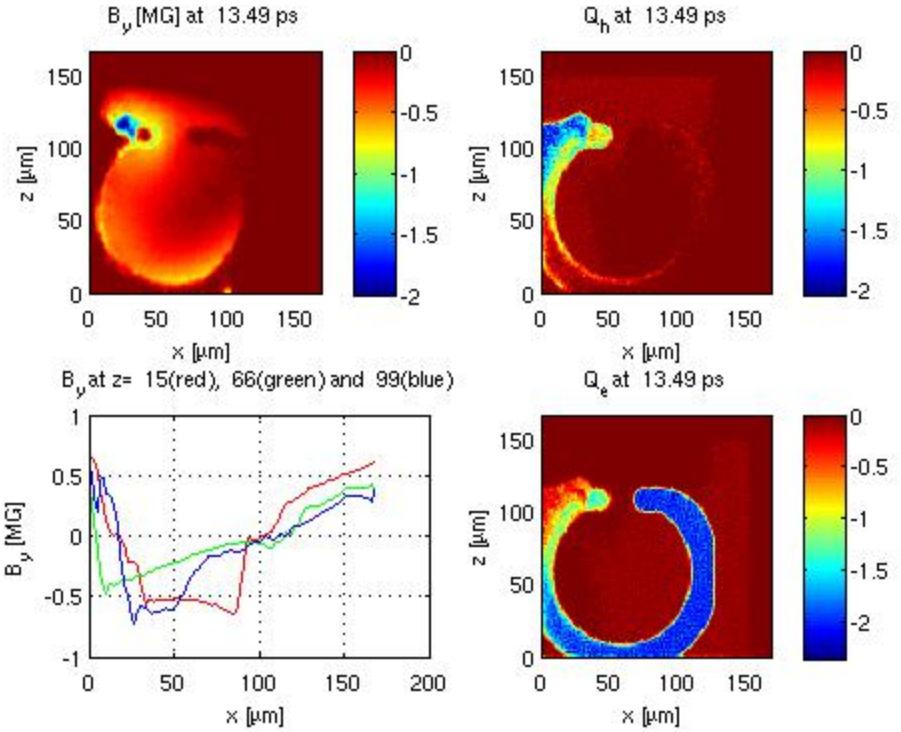

Figure 9. Calculation 2 at 13.5 ps.

The color contour plot in the upper left of Fig. 9 shows electrons and magnetic field moving into the interior low-density region and moving across the gap. The electrons that enter the interior region move down the left side and part of the way up the right side before being lost into the high-density region. Those that jumped the gap propagate along the outer boundary of the high-density region before they, too, are lost into it. The peak magnetic-field value is a modest 0.5 Mg. As before, low-energy hot electrons accumulate in the region close to the accelerator.

At 27 ps, the magnetic-field value has grown slightly as shown in Fig. 10.

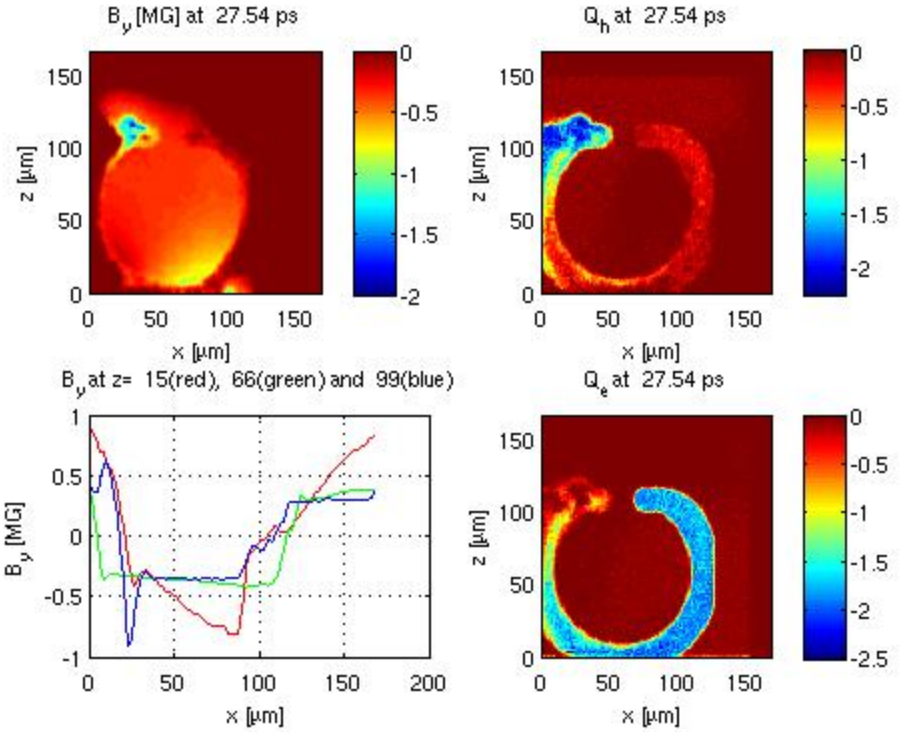

Figure 10. Calculation 2 at 27.5 ps.

The line-outs in the lower-left plot show a slight growth in the magnetic field, but the spread of hot electrons and the elimination of colds throughout the high-density region is even more pronounced. This effect is an artifact of the choice of density of the high-density region.

5. Calculation 2 repeated with 216 particles per cell

We have repeated this calculation with 216 particles per cell. This should reduce the numerical collision frequency and the diffusive transport by a factor of 8. Fig. 11 shows the results at 13.5 ps. Comparing Fig. 11 to Fig. 9, we see that the peak value of the magnetic field has increased as expected. The electrons that entered the interior region now have run up the right side and may be exiting to join those that jumped the gap. And, those that jumped the gap have propagated much farther along the outer boundary of the shell. These results are consistent with a model (discussed in Appendix 3) in which the energy delivered by the laser is balanced against the loss to resistivity in the high-density material.

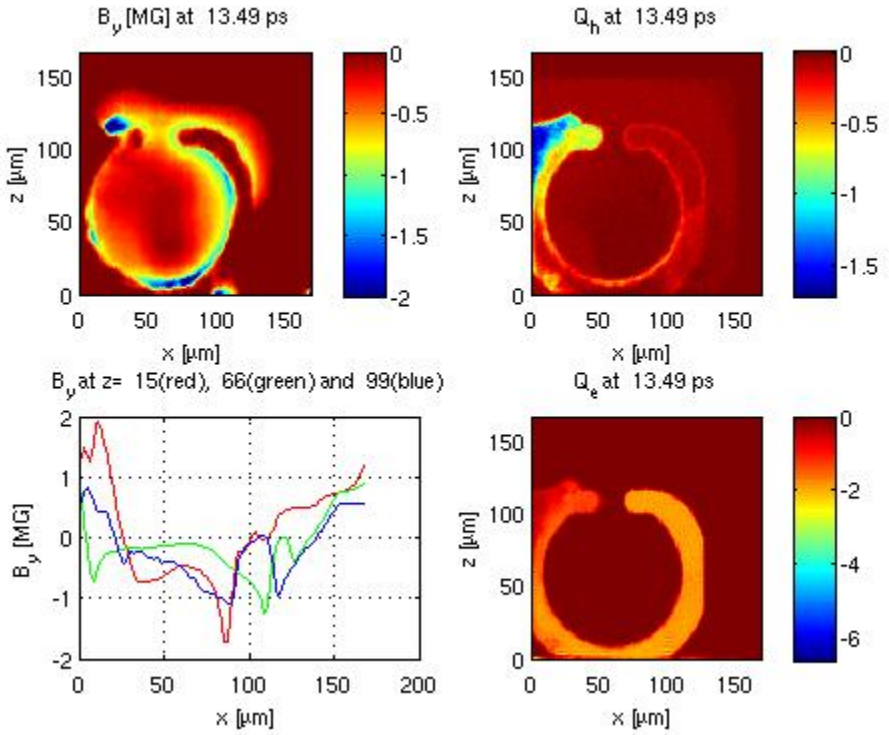

Figure 11. Calculation 2, repeated with 216 particles per cell, at 13.5 ps.

An important feature of the physics in an experiment that is missing in these calculations is the stopping power of the material. Electron ranges for a 20 keV electron, as shown in Table 1, are of the order of 20 μm for intermediate- and high-Z materials. Since the distance from the accelerating region to the interior void is of the order of 20 μm, most of the lower-energy hot electrons in an experiment would be stopped and converted to colds quite close to the accelerating region and the accumulation of colds would be small except near the hot spot.

Material	A	Z	Z*	Mass Density	Electron Density	Collision Frequency	Range
				g cm^{-3}	cm^{-3}	sec^{-1}	μm
Al	27	13	13	2.4	6.9×10^{23}	1.9×10^{12}	54.
Fe	56	26	26	7.1	2.0×10^{24}	5.3×10^{12}	19.
Pd	106	46	38	10.7	2.3×10^{24}	6.2×10^{12}	17.
W	184	74	38	17.0	2.1×10^{24}	5.7×10^{12}	18.

Table 1. The range of an electron with the average energy in a distribution with a temperature of 20 keV is tabulated for four representative materials in the periodic table. The electron density is computed using an effective Z* which is a measure of the number of electrons that are sufficiently weakly bound that an incoming electron can exchange energy with them.

In these calculations, we have used a density of 2×10^{19} cm^{-3} because, although hybrid codes are better at dealing with high density, they are stressed by too high a density. The ion densities in normal materials (and, hence, the electron densities for Z*=1) are much higher as shown in Table 2. The number of hot electrons that are created depends on the intensity of the laser and the pulse length. We have used the correct intensity in these calculations, but have not used a 1 ns pulse length. In a pulse length of 1 ns we will create 20 times as many hot electrons as are created during a time of 50 ps. But, the number of cold electrons, that are available using a real material, increases by a factor of 10^3. Thus, in an experiment of this size, only a tiny fraction of the colds that are available would be converted into hot electrons. In a larger experiment, the fraction of cold electrons converted to hot electrons would be even less.

Material	A	Z	Z*	Mass Density	Ion Density	Plasma Frequency	Collision Frequency
				g cm^{-3}	cm^{-3}	sec^{-1}	sec^{-1}
Al	27	13	1	2.4	5.3×10^{22}	1.3×10^{16}	7.3×10^{16}
Fe	56	26	1	7.1	7.6×10^{22}	1.5×10^{16}	$10.\times10^{16}$
Pd	106	46	1	10.7	6.0×10^{22}	1.4×10^{16}	8.3×10^{16}
W	184	74	1	17.0	5.5×10^{22}	1.3×10^{16}	7.6×10^{16}

Table 2. The ion density (which is equal to the cold-electron density) and the collision frequency seen by an electron in the cold return current are tabulated for four representative materials in the periodic table. Z* is the ionic charge and the number of free electrons per ion. When Z*=1, the electron density is equal to the ion density. A cold electron temperature of 2 eV is assumed.

6. Conclusions

- This magnetic-field generating mechanism is a viable method for generating magnetic fields in ICF targets and for laboratory experiments.

- Useful experiments on material samples can be done with the seed field of 1 to10 Mega-gauss (100 to 1000 Tesla) and higher magnetic fields can be obtained by subsequently compressing the capsule.

- The results reported here can be studied experimentally with a modest CO_2 laser that emits 4.5 J of energy in a 1-ns pulse focused into a 60-μm-diameter spot.

- We have reproduced the published calculation of Forslund and Brackbill [8] and extended them to relativistic energies. The difference in our peak magnetic field (1.25 Mg) versus that in the published calculation (1.3 Mg) is negligible.

- We have shown that hot electrons can jump a gap while the magnetic field penetrates through the gap into an internal region.

- We have shown that hot electrons easily follow both a gently curved *interior* surface and a gently curved *exterior* surface while carrying the magnetic field with them.

- We find that a background plasma or a plasma gradient near the accelerating region is essential to the formation of the magnetic-field structures.

- We find that accelerating the electrons in the direction of their E×B drift does not help. Accelerating them in a cone normal to the surface maximizes the magnetic and electric fields that produce the desired motion.

- We see a substantial accumulation of hot electrons in the interior of the high-density structure. This effect is exaggerated in the calculation because we use an artificially low material-plasma density.

- We see evidence of magnetic-field transport into the high-density material. The transport mechanism may be diffusion caused by numerical collisions or it may be transport of "frozen-in" magnetic field moving with the electrons. .

- The range of 20 keV hot electrons is small compared to reasonable experimental target dimensions. The stopping power of normal materials is not included in the calculations.

- The number of hot electrons created in an experiment is small compared to the number of cold electrons in the target material. This effect is exaggerated in the calculation because of the use of an artificially low material-plasma density.

- Simple estimates of the expected magnetic-field intensity are higher than the observed values in the simulations. This effect may be due to resistive effects from numerical collisions. The effects of resistivity on the return current must be evaluated for experimentally available materials as well.

Acknowledgements

The author would like to thank J. U. Brackbill and G. Lapenta for providing support for the CELESTE code and additional coding for some special capabilities used in this work. This material is based upon work supported by the U. S. Department of Energy, Office of Science, under Award Number DE-FG02-08ER85128.

Appendix 1, Previous Work

In the 1970s and 1980s, little was known about laser-matter interactions and a number of issues were being addressed simultaneously. The absorption of laser light was one of them. Since laser light can only propagate in a plasma whose plasma frequency, $\omega_{pe}{}^2 = n_e e^2 / (\varepsilon_o m_e)$, is less than the laser frequency, the laser light from a CO_2 laser would have to be absorbed at a density 100 times smaller than the density at which light from a Nd-glass laser would be absorbed. At these densities, collisional or inverse-bremstrahlung absorption could not account for the observed absorption. Measurement of x-ray spectra provided the first clue. It was found that the energy ended up in a small number of very energetic hot electrons. With the help of particle-in-cell (PIC) simulation studies, it was concluded that a mechanism called resonant absorption was dominant [6,7]. This mechanism created a large electrostatic wave near the critical surface (where the laser frequency is equal to the plasma frequency) and accelerated electrons away from the dense plasma toward the vacuum. As the first few electrons from the "electron fountain" escaped, an electrostatic field was set up that prevented others from escaping. The electrostatic field returned them to the plasma to generate x-rays and deposit their energy.

Soon after, it was noticed that large numbers of energetic ions were accelerated into the vacuum. Inspection of the target damage showed the expected removal of material from the target surface in a region comparable to the laser spot size, and, in addition, there appeared to be weak surface damage over a circular region centered on the laser spot with a diameter of a few millimeters. Suspicion that laser light, at considerably reduced intensity, was hitting the surface millimeters away from the hot spot either because of focusing errors or some form of scattering was soon dismissed. The explanation of the data again required the use of plasma simulation techniques.

Returning to the "electron fountain" described above, we note that the region from which the electrons are accelerated is bounded. It is most unlikely that the electrons returning to the plasma travel back along the same trajectory that they took when they left. Instead, because of their self field, they are likely to return in a broader pattern. In that case, the returning electrons do not completely cancel the current associated with the escaping electrons and we have a diffuse current loop and its associated magnetic field. The magnetic field is toroidal around the laser hotspot and the electron fountain and its effect on the electrons is to bend their trajectories in such a way as to keep them out of the region occupied by the magnetic field. A hybrid-PIC simulation was needed to verify this model.

The hybrid-PIC simulation code (VENUS) that was available at the time was 2D and Cartesian, so the toroidal B field became anti-parallel fields on either side of a slab electron fountain. Nevertheless, the envisioned B-field was indeed generated [8]. As time progressed, the region occupied by the B-field spread along the outside of the plasma surface while maintaining a fairly constant width and the electrons returned to the plasma at the far end of the B-field region. The electron charge was only partially neutralized by ions as they moved along the outside of the B-field region. The resulting electric field contributed to the electron motion by allowing ExB drift. It also accelerated ions out of the dense plasma of the target surface in a direction normal to the surface of the original plasma. The accelerated ions crossed through the region occupied by the ExB drifting electrons but did not spend enough time there to fully neutralize the electronic charge in the region. Electrons on the outside of the current sheet could easily escape with the ions preventing the build up of electric fields associated with the charging of the target.

This model was consistent with all of the experimental data and quickly became the accepted explanation. Later a cylindrical version of the VENUS code was written [22] and a similar simulation was performed in cylindrical geometry and compared to the Cartesian results. The field obtained in the cylindrical simulation was 0.5 Mgauss at 150 μm from the center of the spot at an intensity of 5×10^{13} W cm^{-2}. The cylindrical version of VENUS was also non-relativistic and incapable of doing the simulation at an intensity of 10^{16} W cm^{-2}.

Appendix 2, Field Strength Estimates

Estimates of the maximum electric current and the magnetic-field strength at the edge of the spot can be obtained using the fact that approximately one third of the laser light is absorbed and converted into a conical relativistic Maxwellian of hot electrons with a temperature that is experimentally measured or taken from the simulations of resonant absorption. The angles, θ_1 and θ_2, are the polar angles of a conical structure. Typically $\theta_1=0^o$ and $\theta_2=20^o$. A relativistic

Maxwellian is obtained by replacing the non-relativistic kinetic energy in the Boltzmann factor in the usual 3D Maxwellian-distribution function with the relativistic kinetic energy and replacing the velocities with the relativistic momenta [16]. K_2 is a modified Bessel function.

$$\frac{J_{zHot}}{n_{Hot} q_e c} = \frac{\cos\theta_1 - \cos\theta_2}{\exp\left(\frac{m_e c^2}{kT_{eHot}}\right) \mathrm{K}_2\left(\frac{m_e c^2}{kT_{eHot}}\right)} \left[\frac{kT_{eHot}}{m_e c^2} + \left(\frac{kT_{eHot}}{m_e c^2}\right)^2 \right]$$

$$\frac{Q_{Hot}}{n_{Hot} m_e c^3} = \frac{2}{\exp\left(\frac{m_e c^2}{kT_{eHot}}\right) \mathrm{K}_2\left(\frac{m_e c^2}{kT_{eHot}}\right)} \left[2\left(\frac{kT_{eHot}}{m_e c^2}\right)^2 + 3\left(\frac{kT_{eHot}}{m_e c^2}\right)^3 \right]$$

$$Q_{Hot} = \eta I$$

For a hot-electron temperature of T_{Hot} = 20 keV, a fractional absorption of η=0.33 and an intensity of I= 5×10^{13} W cm^{-2}, a hot-electron current density of J_{zHot}=2×10^{12} A m^{-2} is obtained. From the radial component of the equation, $\nabla \times B = \mu_o J$, an estimate of the strength of the magnetic field at the outer radius of the hot spot can be obtained.

$$B_\varphi = \frac{1}{2} \mu_o J_{zHot} r_{spot}$$

For a hot-spot radius of 60 μm , a peak magnetic field strength of 150 Tesla or 1.5 Mg is obtained. In the simulation, the observed field strength was 0.5 Mg. This result is consistent with the observation that some of the accelerated electrons returned to the hot spot and did not contribute to the current flowing away by ExB drift. Resistive losses from numerical collisions may also contribute.

In the Helios experiment, a hot-electron temperature of 200 keV was measured at an intensity of 10^{16} W cm^{-2}. At electron energies of 200 keV relativistic corrections are important. Using the relativistic formulae given above to estimate the magnetic field strength in the experiment, a magnetic field strength of 2700 Tesla is obtained. This is a factor of 18 times the peak field at 5×10^{13} W cm^{-2}. If the value of the magnetic field seen in the simulation is multiplied by this factor of 18, an estimate of 900 Tesla or 9 Mg is obtained. These estimates suggest that very interesting magnetic field strengths can be generated by this mechanism.

Appendix 3, B-Field Transport into the High-Density Plasma

To obtain estimates of the transport of the magnetic field into the plasma, we combine Maxwell's equations, neglecting the displacement current, with the equation of motion for the electrons.

$$\nabla \times \vec{E} = -\partial_t \vec{B}$$

$$\nabla \times \vec{B} = \mu_o \vec{J} = -\mu_o n_e e \vec{v}_e$$

$$(\partial_t + \nu)\vec{v}_e = -\frac{e}{m}(\vec{E} + \vec{v}_e \times \vec{B})$$

The result, shown below, is composed of three terms.

$$\left(1 + \nabla \times \frac{c^2}{\omega_{pe}{}^2} \nabla \times\right) \partial_t \vec{B} = -\nabla \times \left(\frac{\nu c^2}{\omega_{pe}{}^2} \nabla \times \vec{B}\right) + \nabla \times (\vec{v}_e \times \vec{B})$$

The factor on the left is associated with the B-field penetration of the plasma to the electromagnetic skin depth on a time scale determined by the displacement current. For singly ionized solid materials of interest, the skin depth is of the order of 0.02 μm. For targets with typical dimensions in the range of 100 μm to 1 mm, this length is negligible and only the first term will be retained. The first term on the right is the usual diffusive transport associated with the material resistivity. The second is the transport of the "frozen-in" field with the electrons as they move. Ignoring, for the moment, the second term, the transport equation becomes the well known diffusion equation.

$$\partial_t \vec{B} = \frac{\nu c^2}{\omega_{pe}{}^2} \nabla^2 \vec{B} = \alpha \nabla^2 \vec{B}$$

We consider a magnetic field with a single component, B_φ, in a vacuum in the region z>0 soaking into a uniform plasma in the region z<0. It is well known that a solution of this problem can be written in terms of the error function.

$$B_\varphi = B_0(r)\left[1 - erf\left(\frac{z}{\sqrt{\alpha t}}\right)\right]$$

Where *erf*(z) for z<0 can be written as

$$erf(z) = \frac{2}{\sqrt{\pi}} \int_z^0 e^{-\xi^2} d\xi$$

We obtain an expression for E_r from Faraday's law.

$$E_r = -\int_{-\infty}^{z} dz' \partial_t B_0(r)\left[1 - erf\left(\frac{z'}{\sqrt{\alpha t}}\right)\right]$$

$$E_r = \frac{1}{2} B_0(r)\left(\frac{\alpha}{\pi t}\right)^{\frac{1}{2}} \exp\left(\frac{-z^2}{\alpha t}\right)$$

And the z component of the Poynting flux vector is given by

$$F_z = \frac{1}{\mu_o}(\vec{E}\times\vec{B})_z = \frac{1}{\mu_o}E_r B_\varphi$$

As the magnetic field diffuses into the cold plasma, it carries with it the energy supplied by the laser. The energy that is transported into a disk shaped surface from $r=r_L$ to $r=r_M$ (r_M is the outer boundary of the region occupied by the magnetic field), is obtained by integrating the Poynting flux over the surface.

$$P_S = 2\pi\int_{r_L}^{r_M} F_z r dr$$

The power transmitted across the surface divided by the laser input power should be less than 1 for a region that the laser can support.

$$\frac{P_S}{\eta I_L \pi r_L^{\,2}} = \frac{\eta I_L r_L^{\,2}}{cfkT_{Hot}}\frac{e^2}{\varepsilon_o fkT_{Hot}}\left(\frac{\nu}{\pi\omega_{pe}^{\,2}t}\right)^{\frac{1}{2}}\ln\left(\frac{r_M}{r_L}\right)\le 1$$

For $\eta I_L = 5\times10^{13}$ Wcm^{-2}, T_{Hot}= 20 keV, r_L=30 μm, a time of 1 ns, an r_M of 1 mm and using the parameters for Fe in Table 2, we obtain

$$\frac{P_S}{\eta I_L \pi r_L^{\,2}} = 0.19$$

And for the Helios experiments, $\eta I_L = 3.33\times10^{15}$ Wcm^{-2}, T_{Hot}= 200 keV, r_L=60 μm, and we obtain

$$\frac{P_S}{\eta I_L \pi r_L^{\,2}} = 0.51$$

These results suggest that the Helios laser and the modest laser that we have used in these calculations can both support the expected magnetic field in a 1-mm size region.

References

1. D.C. Barnes, Scaling relations for high-gain magnetized target fusion systems, Comments on Plasma Phys. and Control. Fusion 18 (1997) 71-84.
2. M.M. Basko, A.J. Kemp, J. Meyer-ter-Vehn, Ignition conditions for magnetized target fusion in cylindrical geometry, Nucl. Fusion 40 (2000) 59-68.
3. R. Betti, Magnetic fields in inertial confinement fusion implosions, High Energy Density Phys., Proc. of the 2nd International Conference on High Energy Density Physics, Austin, Texas, May 2009.
4. M. Borghesi, A.J. MacKinnon, A.R. Bell, R. Gaillard, O. Willi, Megagauss Magnetic Field Generation and Plasma Jet Formation on Solid Targets Irradiated by an Ultraintense Picosecond Laser Pulse, Phys. Rev. Lett. 81 (1998) 112.

5. Jon-Erick Dahlin, Jan Scheffel, Self-consistent, zero-dimensional numerical simulation of a magnetized target fusion configuration, Phys. Scr. 70 (2004) 310-316.
6. D.W. Forslund, J.M. Kindel, K. Lee, E.L. Lindman, R.L. Morse, Theory and Simulation of Resonant Absorption in a Hot Plasma, Phys. Rev. A 11 (1975) 679.
7. D.W. Forslund, J.M. Kindel, K. Lee, Theory of Hot-Electron Spectra at High Laser Intensity, Phys. Rev. Lett. 39 (1977) 284.
8. D.W. Forslund, J.U. Brackbill, Magnetic-Field-Induced Surface Transport on Laser-Irradiated Foils, Phys. Rev. Lett. 48 (1982) 1614.
9. P. Gibbon, E. Forster, Short-pulse laser-plasma interactions, Plasma Phys. Controlled Fusion 38 (1996) 769-793.
10. R.C. Kirkpatrick, I.R. Lindemuth, M.S. Ward, Magnetized Target Fusion -- An Overview, Fusion Technol. 27 (1995) 201-214.
11. Ronald C. Kirkpatrick, Magnetized target fusion for advanced space propulsion, Conf. Proc. 552 (2001) 892-899.
12. R.C. Kirkpatrick, Magnetized target fusion and fusion propulsion, Am. Inst. Phys. Conf. Proc. 608 (2002) 789-792.
13. Ronald C. Kirkpatrick, Fusion reaction product transport for magnetized target fusion, Fusion Sci. and Technol. 52 (2007) 1075-1078.
14. P. Kolodner, E. Yablonovich, Two-Dimensional Distribution of Self-Generated Magnetic Fields near the Laser-Plasma Resonant-Interaction Region, Phys. Rev. Lett. 43 (1979) 1402.
15. G. Lapenta, The Celeste code is an open-source hybrid PIC code that can be found at http://code.google.com/p/celeste
16. R.I. Liboff, Kinetic Theory: Classical, Quantum and Relativistic Descriptions, second ed., John Wiley and Sons, New York, 1998, pp 449-451.
17. D.D. Ryutov, Alpha particles play a relatively minor role in magnetized target fusion systems, Fusion Sci. and Technol. 41 (2002) 88-91.
18. D.D. Ryutov, Y.F. Thio, Solving the standoff problem for magnetized target fusion: plasma streams as disposable electrodes, plus a local spherical blanket, Fusion Eng. and Des. 26 (2006) 173.
19. Y. Sakagami, H. Kawakami, S. Nagao, C. Yamanaka, Two-Dimensional Distribution of Self-Generated Magnetic Fields near the Laser-Plasma Resonant-Interaction Region, Phys. Rev. Lett. 42 (1979) 839.
20. U. Wagner, M. Tatarakis, A. Gopal, F.N. Beg, E.L. Clark, A.E. Dangor, R.G. Evans, M.G. Haines, S.P.D. Mangles, P.A. Norreys, M.-S. Wei, M. Zepf, K. Krushelnick, Laboratory measurements of 0.7 GG magnetic fields generated during high-intensity laser interactions with dense plasmas, Phys. Rev. E 70 (2004) 026401.
21. Jon M. Wallace, Nonlocal Energy Deposition in High-Intensity Laser-Plasma Interactions, Phys. Rev. Lett. 55 (1985) 707.
22. Jon M. Wallace, J.U. Brackbill, D.W. Forslund, An Implicit Moment Electromagnetic Plasma Simulation in Cylindrical Coordinates," J. Comput. Phys. 63 (1986) 434.
23. M.A. Yates, D.B. van Hulsteyn, H. Rutkowski, G. Kyrala, J.U. Brackbill, Experimental Evidence for Self-Generated Magnetic Fields and Remote Energy Deposition in Laser-Irradiated Targets, Phys. Rev. Lett. 49 (1982) 1702.